Progress In Electromagnetics Research M, Vol. 100, 35–50, 2021

A Novel Analytical Method Suitable for Coupled Electromagnetic Field of Circuit

Rui Zhang[1, *], Yibo Wang[2], and Honghua Xu[2]

Abstract—A novel analytical method suitable for coupled electromagnetic field of a circuit is proposed in this paper. In a high frequency circuit and high-frequency converter, skin effects are obvious, and the variations in resistance and inductance values depend on frequency. In addition, the voltage and current distribution changes of a high frequency circuit generated with a high-frequency converter during dynamic switching process are complicated and depend on time. A novel analytical method suitable for coupled electromagnetic field of circuit in parameter optimization design of high-frequency circuit and high-frequency converter is proposed in this paper. The proposed method considers the influence of skin effect and coupled electromagnetic field on parameter variation simultaneously. According to the law between parameter variation and line length, the calculation process of parameter optimization will be simpler and more effective.

1. INTRODUCTION

Multiphysics analysis has become an analytical method widely used in various research fields. The electromagnetic coupling relationship of space multiphysics can be represented by a series of Maxwell's equations.

In high frequency circuit, eddy current phenomena are common [1], and skin effect and proximity effect are obvious [2, 3]. When a conductor size is larger than the skin depth δ, the change of resistance and inductance values depends on frequency. The accurate prediction of eddy current loss and current and voltage distribution with skin effect are important [4, 5]. In addition, the multi-physics analysis of high frequency converter system is becoming more important in improving efficiency and reliability. Among them, the relationship between multi-physics and skin effect caused by transient voltage and current changes is an important problem to be solved [6, 7]. In the process of analysis, PEEC model and finite-element method are proposed for skin effect [8, 9].

In a high-frequency circuit and high-frequency converter, dynamic switching process can cause complex electromagnetic coupling relationship and circuit parameter changes, and traditional skin effect formulas are not applicable.

Thus, some novel circuit model analytical methods are proposed [10–13]. A dual-loop model based on boost and buck converter is proposed, and the steady-state field of typical frequency point is simulated in frequency domain [14]. However, the distribution law of high frequency electromagnetic field cannot be used to accurately optimize loop parameters.

So a simplified calculation method of resistance and inductance parameter optimization considering the influence of high frequency electromagnetic field needs to be proposed in order to balance complex voltage and current changes in circuits.

Received 29 July 2020, Accepted 14 October 2020, Scheduled 27 December 2020

* Corresponding author: Rui Zhang (zr@mail.iee.ac.cn).

[1] Institute of Electrical Engineering, Chinese Academy of Sciences, University of Chinese Academy of Sciences, Beijing, China.

[2] Institute of Electrical Engineering, Chinese Academy of Sciences, Beijing, China.

For a high-frequency circuit, complex voltage and current changes caused by the variations in line impedance value depend on frequency and skin effect. For a high-frequency converter, complex voltage and current changes are caused by complex coupling electromagnetic field in dynamic switching process.

2. COUPLED ELECTROMAGNETIC FIELD OF CIRCUIT

Maxwell's equations represent a complex electromagnetic coupling relationship in conductors and circuits. It can be seen from Equation (1) that the coupling relationship is related to both circuit frequency and field parameters. On the contrary, conductor and circuit parameter optimization can be solved based on the influence of frequency and space electromagnetic field on the conductor and circuit.

$$\begin{cases} curl\mathbf{H}= \mathbf{J}+\dfrac{\partial \mathbf{D}}{\partial t} \\ \nabla \times \mathbf{H} = \mathbf{J} + \dfrac{\partial \mathbf{D}}{\partial t} \\ div\mathbf{D} =\rho \\ \nabla \cdot \mathbf{D} = \rho \end{cases} \quad \begin{cases} curl\mathbf{E}= -\dfrac{\partial \mathbf{B}}{\partial t} \\ \nabla \times \mathbf{E} = -\dfrac{\partial \mathbf{B}}{\partial t} \\ div\mathbf{B} = 0 \\ \nabla \cdot \mathbf{B} = 0 \end{cases} \quad \begin{cases} \mathbf{D} = \varepsilon \mathbf{E} \\ \mathbf{B} = \mu \mathbf{H} \\ \mathbf{J} = \sigma \mathbf{E} \end{cases} \tag{1}$$

where $\mathbf{E}$ indicates the electric field, $\mathbf{H}$ the magnetic field, $\mathbf{D}$ the electric flux density, $\mathbf{B}$ the magnetic flux density, $\mathbf{J}$ the current density, ε the dielectric constant, σ the conductivity, and μ the permeability. Equation (1) uses two symbolic expressions to illustrate the complex electromagnetic field relationship.

Available from Equation (1),

$$\begin{cases} \nabla \times \mathbf{H}(\mathbf{r},t) = \sigma \mathbf{E}(\mathbf{r},t) + \dfrac{\partial \varepsilon \mathbf{E}(\mathbf{r},t)}{\partial t} \\ \nabla \times \mathbf{E}(\mathbf{r},t) = -\dfrac{\partial \mu \mathbf{H}(\mathbf{r},t)}{\partial t} \\ \nabla \times \nabla \times \mathbf{E}(\mathbf{r},t) = -\sigma\mu \dfrac{\partial \mathbf{E}(\mathbf{r},t)}{\partial t} - \varepsilon\mu \dfrac{\partial^2 \mathbf{E}(\mathbf{r},t)}{\partial t^2} \\ \nabla \times \nabla \times \mathbf{H}(\mathbf{r},t) = -\sigma\mu \dfrac{\partial \mathbf{H}(\mathbf{r},t)}{\partial t} - \varepsilon\mu \dfrac{\partial^2 \mathbf{H}(\mathbf{r},t)}{\partial t^2} \end{cases} \tag{2}$$

$\mathbf{E}(\mathbf{r},t)$ and $\mathbf{H}(\mathbf{r},t)$ are related to vector radius and time.

Define a closed circuit loop l_1 and coordinates x, y, z in Fig. 1 [14].

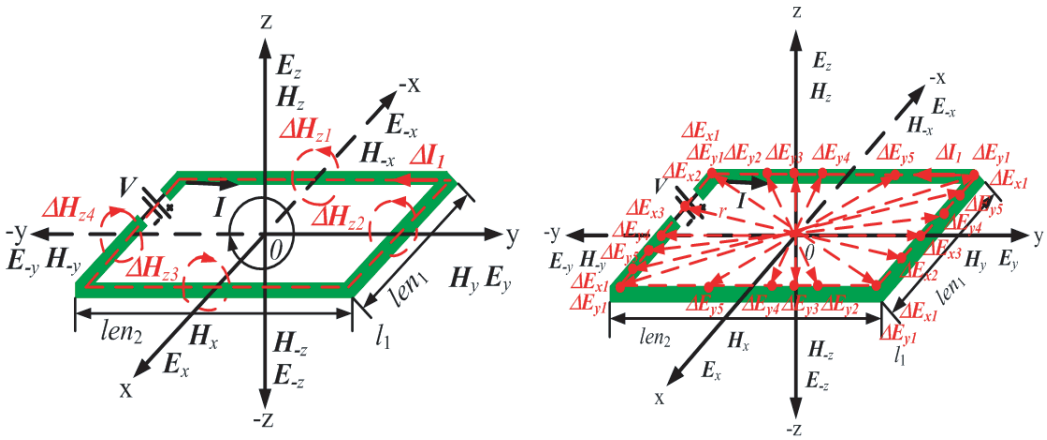

Figure 1. Space electromagnetic field distribution of a circuit loop.

The dynamic voltage added in l_1 is V, and the dynamic current flowing through l_1 is I. The components of electric and magnetic field vector on coordinate axis are: $\mathbf{E_x}$, $\mathbf{E_y}$, $\mathbf{E_z}$, $\mathbf{E_{-x}}$, $\mathbf{E_{-y}}$, $\mathbf{E_{-z}}$ and $\mathbf{H_x}$, $\mathbf{H_y}$, $\mathbf{H_z}$, $\mathbf{H_{-x}}$, $\mathbf{H_{-y}}$, $\mathbf{H_{-z}}$. In Fig. 1, the center coordinate of l_1 is 0, and the induced magnetic field in center has a symmetrical and radial effect on l_1, such as $\mathbf{\Delta H_{z1}}$–$\mathbf{z4}$, $\mathbf{\Delta I_1}$. The change of

induced magnetic field causes the change of induced electric field, such as $\Delta\mathbf{E_{x1-x5}}$, $\Delta\mathbf{E_{y1-y5}}$. In l_1, $-len1/2 \leqq x \leqq len1/2$, $-len2/2 \leqq y \leqq len2/2$.

Equation (2) can be converted to numerical calculation expression,

$$\begin{cases} \dfrac{\partial^2 \mathbf{E}(\mathbf{r},t)}{\partial \mathbf{r}^2} = \sigma\mu \dfrac{\partial \mathbf{E}(\mathbf{r},t)}{\partial t} + \varepsilon\mu \dfrac{\partial^2 \mathbf{E}(\mathbf{r},t)}{\partial t^2} \\ \dfrac{\partial^2 \mathbf{H}(\mathbf{r},t)}{\partial \mathbf{r}^2} = \sigma\mu \dfrac{\partial \mathbf{H}(\mathbf{r},t)}{\partial t} + \varepsilon\mu \dfrac{\partial^2 \mathbf{H}(\mathbf{r},t)}{\partial t^2} \end{cases} \tag{3}$$

Assuming $\mathbf{E}(\mathbf{r},0) = \mathbf{H}(\mathbf{r},0) = 0$, the Laplace transform of Equation (3) is,

$$\begin{cases} \dfrac{\partial^2 \mathbf{E}(\mathbf{r},s)}{\partial \mathbf{r}^2} = \left(\sigma\mu s + \varepsilon\mu s^2\right)\mathbf{E}(\mathbf{r},s) \\ \dfrac{\partial^2 \mathbf{H}(\mathbf{r},s)}{\partial \mathbf{r}^2} = \left(\sigma\mu s + \varepsilon\mu s^2\right)\mathbf{H}(\mathbf{r},s) \end{cases} \tag{4}$$

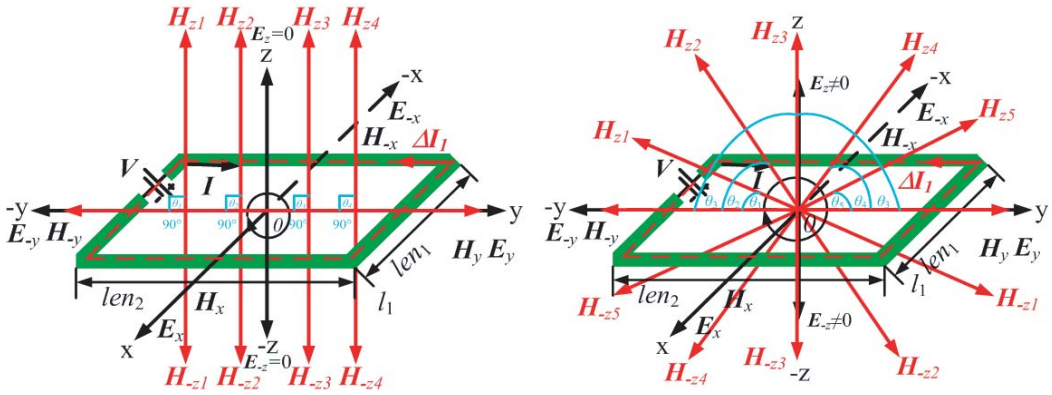

Figure 2. Different incident angles of $\mathbf{H_Z}$ with $\mathbf{E_z} = 0$ and $\mathbf{E_z} \neq 0$.

In Fig. 2, when $\mathbf{H_z}(\mathbf{r},s) \neq 0$, it is incident perpendicularly from above the center of the plane loop l_1, which is $\theta = 90°$ with respect to the plane loop l_1. Due to the symmetry of $\mathbf{E}(\mathbf{r},s) = \mathbf{E}(-\mathbf{r},s)$ and $\mathbf{H}(\mathbf{r},s) = \mathbf{H}(-\mathbf{r},s)$, the boundary conditions in l_1: $\mathbf{E_z}(\mathbf{r},s) = 0$, $|x| - |y| \neq 0$, $\theta = 90°$, $-len1/2 \leqq x \leqq len1/2$, $-len2/2 \leqq y \leqq len2/2$, solve $\mathbf{E}(\mathbf{r},s)$ and $\mathbf{H}(\mathbf{r},s)$, where a_1 and b_1 are related to the incident angle θ in Equation (5),

$$\begin{cases} \mathbf{E}(\mathbf{r},s) = 2a_1 \cosh\left(\sqrt{\sigma\mu s + \varepsilon\mu s^2}\cdot\sqrt{x^2+y^2+z^2}\right)\cdot\hat{\mathbf{r}},\ a_1 = A_1\sin\theta,\ \theta = 90° \\ \mathbf{H}(\mathbf{r},s) = 2b_1 \cosh\left(\sqrt{\sigma\mu s + \varepsilon\mu s^2}\cdot\sqrt{x^2+y^2+z^2}\right)\cdot\hat{\mathbf{r}},\ b_1 = B_1\sin\theta,\ \theta = 90° \\ \mathbf{E}(\mathbf{r},s) = \mathbf{E}_x(r,s)\,\hat{\mathbf{x}} + \mathbf{E}_y(r,s)\,\hat{\mathbf{y}} + \mathbf{E}_z(r,s)\,\hat{\mathbf{z}} \\ \mathbf{H}(\mathbf{r},s) = \mathbf{H}_x(r,s)\,\hat{\mathbf{x}} + \mathbf{H}_y(r,s)\,\hat{\mathbf{y}} + \mathbf{H}_z(r,s)\,\hat{\mathbf{z}} \\ \mathbf{E_z}(\mathbf{r},s) = 0 \end{cases} \tag{5}$$

$$\begin{cases} \nabla\times\mathbf{H}(\mathbf{r},s) = \left(\dfrac{\partial \mathbf{H}_z(r,s)}{\partial y} - \dfrac{\partial \mathbf{H}_y(r,s)}{\partial z}\right)\hat{\mathbf{x}} + \left(\dfrac{\partial \mathbf{H}_x(r,s)}{\partial z} - \dfrac{\partial \mathbf{H}_z(r,s)}{\partial x}\right)\hat{\mathbf{y}} + \left(\dfrac{\partial \mathbf{H}_y(r,s)}{\partial x} - \dfrac{\partial \mathbf{H}_x(r,s)}{\partial y}\right)\hat{\mathbf{z}} \\ \qquad\qquad = (\sigma + \varepsilon s)\left(\mathbf{E}_x(r,s)\,\hat{\mathbf{x}} + \mathbf{E}_y(r,s)\,\hat{\mathbf{y}} + \mathbf{E}_z(r,s)\,\hat{\mathbf{z}}\right) \\ \nabla\times\mathbf{E}(\mathbf{r},s) = \left(\dfrac{\partial \mathbf{E}_z(r,s)}{\partial y} - \dfrac{\partial \mathbf{E}_y(r,s)}{\partial z}\right)\hat{\mathbf{x}} + \left(\dfrac{\partial \mathbf{E}_x(r,s)}{\partial z} - \dfrac{\partial \mathbf{E}_z(r,s)}{\partial x}\right)\hat{\mathbf{y}} + \left(\dfrac{\partial \mathbf{E}_y(r,s)}{\partial x} - \dfrac{\partial \mathbf{E}_x(r,s)}{\partial y}\right)\hat{\mathbf{z}} \\ \qquad\qquad = -\mu s\left(\mathbf{H}_x(r,s)\hat{\mathbf{x}} + \mathbf{H}_y(r,s)\,\hat{\mathbf{y}} + \mathbf{H}_z(r,s)\,\hat{\mathbf{z}}\right) \end{cases} \tag{6}$$

In Equation (7), $\mathbf{E_x}$, $\mathbf{E_y}$, $\mathbf{E_z}$ and $\mathbf{H_x}$, $\mathbf{H_y}$, $\mathbf{H_z}$ can be represented using Eqs. (5), (6). The change increments affected by induced magnetic field and electric field are also obtained.

$$\begin{cases} \dfrac{\partial \mathbf{H}_z(r,s)}{\partial y} - \dfrac{\partial \mathbf{H}_y(r,s)}{\partial z} = -2B_1 \dfrac{\sqrt{\sigma\mu s + \varepsilon\mu s^2}\,(|y|-|z|)}{r} \sinh\left(\sqrt{\sigma\mu s + \varepsilon\mu s^2} r\right) = (\sigma + \varepsilon s)\,\mathbf{E}_x(r,s) \\ \dfrac{\partial \mathbf{H}_x(r,s)}{\partial z} - \dfrac{\partial \mathbf{H}_z(r,s)}{\partial x} = -2B_1 \dfrac{\sqrt{\sigma\mu s + \varepsilon\mu s^2}\,(|z|-|x|)}{r} \sinh\left(\sqrt{\sigma\mu s + \varepsilon\mu s^2} r\right) = (\sigma + \varepsilon s)\,\mathbf{E}_y(r,s) \\ \dfrac{\partial \mathbf{H}_y(r,s)}{\partial x} - \dfrac{\partial \mathbf{H}_x(r,s)}{\partial y} = (\sigma + \varepsilon s)\,\mathbf{E}_z(r,s) = 0 \\ \dfrac{\partial \mathbf{E}_z(r,s)}{\partial y} - \dfrac{\partial \mathbf{E}_y(r,s)}{\partial z} = 2A_1 \dfrac{\sqrt{\sigma\mu s + \varepsilon\mu s^2}\,|z|}{r} \sinh\left(\sqrt{\sigma\mu s + \varepsilon\mu s^2} r\right) = -\mu s \mathbf{H}_x(r,s) \\ \dfrac{\partial \mathbf{E}_x(r,s)}{\partial z} - \dfrac{\partial \mathbf{E}_z(r,s)}{\partial x} = -2A_1 \dfrac{\sqrt{\sigma\mu s + \varepsilon\mu s^2}\,|z|}{r} \sinh\left(\sqrt{\sigma\mu s + \varepsilon\mu s^2} r\right) = -\mu s \mathbf{H}_y(r,s) \\ \dfrac{\partial \mathbf{E}_y(r,s)}{\partial x} - \frac{\partial \mathbf{E}_x(r,s)}{\partial y} = -2A_1 \dfrac{\sqrt{\sigma\mu s + \varepsilon\mu s^2}\,(|x|-|y|)}{r} \sinh\left(\sqrt{\sigma\mu s + \varepsilon\mu s^2} r\right) = -\mu s \mathbf{H}_z(r,s) \end{cases} \tag{7}$$

$$\begin{cases} \mathbf{E}_x(r,s) = -2B_1 \dfrac{\sqrt{\sigma\mu s + \varepsilon\mu s^2}\,(|y|-|z|)}{(\sigma + \varepsilon s)\,r} \sinh\left(\sqrt{\sigma\mu s + \varepsilon\mu s^2} r\right) \\ \mathbf{E}_y(r,s) = -2B_1 \dfrac{\sqrt{\sigma\mu s + \varepsilon\mu s^2}\,(|z|-|x|)}{(\sigma + \varepsilon s)\,r} \sinh\left(\sqrt{\sigma\mu s + \varepsilon\mu s^2} r\right) \\ \mathbf{E}_z(r,s) = 0 \\ \mathbf{H}_x(r,s) = 2A_1 \dfrac{\sqrt{\sigma\mu s + \varepsilon\mu s^2}\,|z|}{-\mu s r} \sinh\left(\sqrt{\sigma\mu s + \varepsilon\mu s^2} r\right) \\ \mathbf{H}_y(r,s) = 2A_1 \dfrac{\sqrt{\sigma\mu s + \varepsilon\mu s^2}\,|z|}{\mu s r} \sinh\left(\sqrt{\sigma\mu s + \varepsilon\mu s^2} r\right) \\ \mathbf{H}_z(r,s) = 2A_1 \dfrac{\sqrt{\sigma\mu s + \varepsilon\mu s^2}\,(|x|-|y|)}{\mu s r} \sinh\left(\sqrt{\sigma\mu s + \varepsilon\mu s^2} r\right) \end{cases} \tag{8}$$

When $\mathbf{H_z}(\mathbf{r},s) \neq 0$ and $0 < \theta < 90^\circ$ with respect to the plane loop l_1, due to $\theta \neq 90^\circ$, $\mathbf{H_x}$, $\mathbf{H_y}$ and $\mathbf{E_z}$ will change so that the symmetry of $\mathbf{E}(\mathbf{r},s)$ and $\mathbf{H}(\mathbf{r},s)$ will also change. The boundary conditions in l_1: $\mathbf{E_z}(\mathbf{r},s) \neq 0$, $|x| - |y| \neq 0$, $0 < \theta < 90^\circ$, $-len1/2 \leqq x \leqq len1/2$, $-len2/2 \leqq y \leqq len2/2$, solve $\mathbf{E}(\mathbf{r},s)$ and $\mathbf{H}(\mathbf{r},s)$, where a_1 and b_1 are related to the incident angle θ in Equation (9),

$$\begin{cases} \mathbf{E}_x(r,s) = -2B_1 \sin\theta \dfrac{\sqrt{\sigma\mu s + \varepsilon\mu s^2}\,(|y|-|z|)}{(\sigma + \varepsilon s)\,r} \sinh\left(\sqrt{\sigma\mu s + \varepsilon\mu s^2} r\right),\ 0^\circ < \theta < 90^\circ \\ \mathbf{E}_y(r,s) = -2B_1 \sin\theta \dfrac{\sqrt{\sigma\mu s + \varepsilon\mu s^2}\,(|z|-|x|)}{(\sigma + \varepsilon s)\,r} \sinh\left(\sqrt{\sigma\mu s + \varepsilon\mu s^2} r\right),\ 0^\circ < \theta < 90^\circ \\ \mathbf{E}_z(r,s) = -2B_1 \cos\theta \dfrac{\sqrt{\sigma\mu s + \varepsilon\mu s^2}\,(|x|-|y|)}{(\sigma + \varepsilon s)\,r} \sinh\left(\sqrt{\sigma\mu s + \varepsilon\mu s^2} r\right),\ 0^\circ < \theta < 90^\circ \\ \mathbf{H}_x(r,s) = 2A_1 \dfrac{\sqrt{\sigma\mu s + \varepsilon\mu s^2}\,|z|}{-\mu s r} \sinh\left(\sqrt{\sigma\mu s + \varepsilon\mu s^2} r\right) \\ \qquad\qquad +2A_1 \cos\theta \dfrac{\sqrt{\sigma\mu s + \varepsilon\mu s^2}(|y|)}{\mu s r} \sinh\left(\sqrt{\sigma\mu s + \varepsilon\mu s^2} r\right),\ 0^\circ < \theta < 90^\circ \\ \mathbf{H}_y(r,s) = 2A_1 \dfrac{\sqrt{\sigma\mu s + \varepsilon\mu s^2}\,|z|}{\mu s r} \sinh\left(\sqrt{\sigma\mu s + \varepsilon\mu s^2} r\right) \\ \qquad\qquad -2A_1 \cos\theta \dfrac{\sqrt{\sigma\mu s + \varepsilon\mu s^2}(|x|)}{\mu s r} \sinh\left(\sqrt{\sigma\mu s + \varepsilon\mu s^2} r\right),\ 0^\circ < \theta < 90^\circ \\ \mathbf{H}_z(r,s) = 2A_1 \sin\theta \dfrac{\sqrt{\sigma\mu s + \varepsilon\mu s^2}\,(|x|-|y|)}{\mu s r} \sinh\left(\sqrt{\sigma\mu s + \varepsilon\mu s^2} r\right),\ 0^\circ < \theta < 90^\circ \end{cases} \tag{9}$$

$$
\begin{cases}
0< \mathbf{E}_x(r,s) = -2B_1 \sin\theta \dfrac{\sqrt{\sigma\mu s+\varepsilon\mu s^2}\,(|y|-|z|)}{(\sigma+\varepsilon s)\,r} \sinh\left(\sqrt{\sigma\mu s+\varepsilon\mu s^2}r\right) \\
\qquad < -2B_1 \dfrac{\sqrt{\sigma\mu s+\varepsilon\mu s^2}\,(|y|-|z|)}{(\sigma+\varepsilon s)\,r} \sinh\left(\sqrt{\sigma\mu s+\varepsilon\mu s^2}r\right) \\
0< \mathbf{E}_y(r,s) = -2B_1 \sin\theta \dfrac{\sqrt{\sigma\mu s+\varepsilon\mu s^2}\,(|z|-|x|)}{(\sigma+\varepsilon s)\,r} \sinh\left(\sqrt{\sigma\mu s+\varepsilon\mu s^2}r\right) \\
\qquad < -2B_1 \dfrac{\sqrt{\sigma\mu s+\varepsilon\mu s^2}\,(|z|-|x|)}{(\sigma+\varepsilon s)\,r} \sinh\left(\sqrt{\sigma\mu s+\varepsilon\mu s^2}r\right) \\
0< \mathbf{E}_z(r,s) = -2B_1 \cos\theta \dfrac{\sqrt{\sigma\mu s+\varepsilon\mu s^2}\,(|x|-|y|)}{(\sigma+\varepsilon s)\,r} \sinh\left(\sqrt{\sigma\mu s+\varepsilon\mu s^2}r\right) \\
\qquad < -2B_1 \dfrac{\sqrt{\sigma\mu s+\varepsilon\mu s^2}\,(|x|-|y|)}{(\sigma+\varepsilon s)\,r} \sinh\left(\sqrt{\sigma\mu s+\varepsilon\mu s^2}r\right) \\
-2A_1 \dfrac{\sqrt{\sigma\mu s+\varepsilon\mu s^2}\,|z|}{\mu s r} \sinh\left(\sqrt{\sigma\mu s+\varepsilon\mu s^2}r\right) < \mathbf{H}_x(r,s) \\
= 2A_1 \dfrac{\sqrt{\sigma\mu s+\varepsilon\mu s^2}\,|z|}{-\mu s r} \sinh\left(\sqrt{\sigma\mu s+\varepsilon\mu s^2}r\right) + 2A_1 \cos\theta \dfrac{\sqrt{\sigma\mu s+\varepsilon\mu s^2}(|y|)}{\mu s r} \sinh\left(\sqrt{\sigma\mu s+\varepsilon\mu s^2}r\right) \\
< 2A_1 \dfrac{\sqrt{\sigma\mu s+\varepsilon\mu s^2}(|y|-|z|)}{\mu s r} \sinh\left(\sqrt{\sigma\mu s+\varepsilon\mu s^2}r\right) \\
2A_1 \dfrac{\sqrt{\sigma\mu s+\varepsilon\mu s^2}\,(|z|-|x|)}{\mu s r} \sinh\left(\sqrt{\sigma\mu s+\varepsilon\mu s^2}r\right) < \mathbf{H}_y(r,s) \\
= 2A_1 \dfrac{\sqrt{\sigma\mu s+\varepsilon\mu s^2}\,|z|}{\mu s r} \sinh\left(\sqrt{\sigma\mu s+\varepsilon\mu s^2}r\right) - 2A_1 \cos\theta \dfrac{\sqrt{\sigma\mu s+\varepsilon\mu s^2}(|x|)}{\mu s r} \sinh\left(\sqrt{\sigma\mu s+\varepsilon\mu s^2}r\right) \\
<2A_1 \dfrac{\sqrt{\sigma\mu s+\varepsilon\mu s^2}\,|z|}{\mu s r} \sinh\left(\sqrt{\sigma\mu s+\varepsilon\mu s^2}r\right) \\
0< \mathbf{H}_z(r,s) = 2A_1 \sin\theta \dfrac{\sqrt{\sigma\mu s+\varepsilon\mu s^2}\,(|x|-|y|)}{\mu s r} \sinh\left(\sqrt{\sigma\mu s+\varepsilon\mu s^2}r\right) \\
\qquad <2A_1 \dfrac{\sqrt{\sigma\mu s+\varepsilon\mu s^2}\,(|x|-|y|)}{\mu s r} \sinh\left(\sqrt{\sigma\mu s+\varepsilon\mu s^2}r\right)
\end{cases}
\tag{10}
$$

Assuming in l_1, the initial value of applied dynamic voltage is V_0, and the initial value of applied dynamic current is I_0,

$$
\begin{cases}
\oint_{l_1} \left(\mathbf{E_x}(\mathbf{r},s) + \mathbf{E_y}(\mathbf{r},s)\right) dl_1 = \text{-}\Delta V \\
\oint_{l} \mathbf{H_z}(\mathbf{r},s) dl = -\Delta I \\
V^* = V_0\text{-}\Delta V \\
I^* = I_0\text{-}\Delta I \\
Z^* = V^*/I^*
\end{cases}
\tag{11}
$$

According to Equations (8)–(11), the variation of voltage and current, and the variation of line impedance with frequency caused by space electromagnetic field distribution of l_1 can also be obtained.

The current through a cylindrical conductor with radius r_c can be expressed as [1],

$$
I(s) = \frac{\pi r_c}{2}\sigma \int_{-r_c}^{r_c} E(r,s)\,dr = \frac{2\pi r_c a_1 \sigma}{\sqrt{\sigma\mu s+\varepsilon\mu s^2}} \sinh\left(\sqrt{\sigma\mu s+\varepsilon\mu s^2}\cdot r_c\right) \tag{12}
$$

The voltage $V(s)$ across conductor is $V(s) = E(r_c, s)l$, and the impedance value of conductor is $Z(s)$,

$$Z(s) = \frac{V(s)}{I(s)} = \frac{2a_1 \cosh\left(\sqrt{\sigma\mu s + \varepsilon\mu s^2} \cdot r_c\right) l}{\frac{2\pi r_c a_1 \sigma}{\sqrt{\sigma\mu s + \varepsilon\mu s^2}} \sinh\left(\sqrt{\sigma\mu s + \varepsilon\mu s^2} \cdot r_c\right)}$$

$$= \underbrace{\frac{l}{\pi r_c^2 \sigma}}_{R_0} \cdot \underbrace{\sqrt{\sigma\mu s + \varepsilon\mu s^2} r_c}_{\lambda} \coth\left(\underbrace{\sqrt{\sigma\mu s + \varepsilon\mu s^2} \cdot r_c}_{\lambda}\right) \tag{13}$$

$$\lambda \coth \lambda = 1 + \lambda^2/3 - \lambda^4/45 + 2\lambda^6/945 - \lambda^8/4725 + \cdots = \sum_{\theta=0}^{\infty} \frac{2^{2\theta} B_{2\theta}}{(2\theta)!} \lambda^{2\theta} \tag{14}$$

When variable λ is introduced, $Z(s)$ can be converted into the form of Equation (16). $B_{2\theta}$ is Bernoulli number as Equation (15).

$$\frac{z}{e^z - 1} = \sum_{\theta=0}^{\infty} \frac{B_\theta z^\theta}{\theta!} \tag{15}$$

where $B_0 = 1$, $B_1 = -1/2$, $B_2 = 1/6$, $B_3 = 0$, $B_4 = -1/30$, $B_5 = 0$, $B_6 = 1/42$, $B_7 = 0$, $B_8 = -1/30$, $B_9 = 0$, $B_{10} = 5/66$, $B_{11} = 0$, $B_{12} = -691/2730$, $B_{13} = 0$, $B_{14} = 6/7$, $B_{15} = 0$, $B_{16} = -3617/510$.

When $s = 0$, DC resistance $R_0 = l/\pi r_c^2 \sigma$, characteristic frequency $\omega_c = 1/\mu\sigma$ make $\beta = \omega/\omega_c$. If $\beta = \omega/\omega_c = 1$ and $\varepsilon = 0$ at high frequency, λ is,

$$\begin{cases} \lambda = \sqrt{\sigma\mu s + \varepsilon\mu s^2} r_c = \sqrt{\left(j\dfrac{\omega}{\frac{1}{\sigma\mu}} - \dfrac{\varepsilon}{\sigma^2\mu}\left(\dfrac{\omega}{\frac{1}{\sigma\mu}}\right)^2\right)} r_c = \sqrt{\left(j\dfrac{\omega}{\omega_c} - \dfrac{\varepsilon}{\sigma^2\mu}\left(\dfrac{\omega}{\omega_c}\right)^2\right)} r_c \\ \quad = \sqrt{\left(j\beta - \dfrac{\varepsilon}{\sigma^2\mu}\beta^2\right)} r_c, \left(\omega_c = \dfrac{1}{\sigma\mu}, \beta = \dfrac{\omega}{\omega_c}\right) \\ Z(j\omega_c)/R_0 = 1 + r_c^2 j/3 + r_c^4/45 = 1.0222 r_c^4 + j0.3333 r_c^2 \ (\varepsilon = 0) \\ Z(j\beta)/R_0 = R/R_0 + jX/R_0 \end{cases} \tag{16}$$

Table 1 shows the changes in impedance value at different frequency ratios β.

Table 1. Impedance value for cylindrical conductor with radius r_c.

Frequency ratio β	Various impedance value
$\beta = 1$	$1.0222 r_c^4 + 0.3333_c^2$
$\beta = 5$	$1.5555 r_c^4 + j1.6665 r_c^2$
$\beta = 10$	$3.2222 r_c^4 + j3.3333 r_c^2$
$\beta = 20$	$9.8888 r_c^4 + j6.6666 r_c^2$
$\beta = 50$	$56.5555 r_c^4 + j16.665 r_c^2$

As shown in Fig. 3 and Table 1, for a cylindrical conductor with radius r_c, when $\beta \leqq 10$, R/R, and X/R tend to be equal; the gap between R/R and X/R increases when $\beta \geqq 10$, and the trend of resistance ratio R/R gradually increases when $\beta \geqq 20$. It can be seen that the impedance value has different changing trends at different frequency ratios β and different radii r_c.

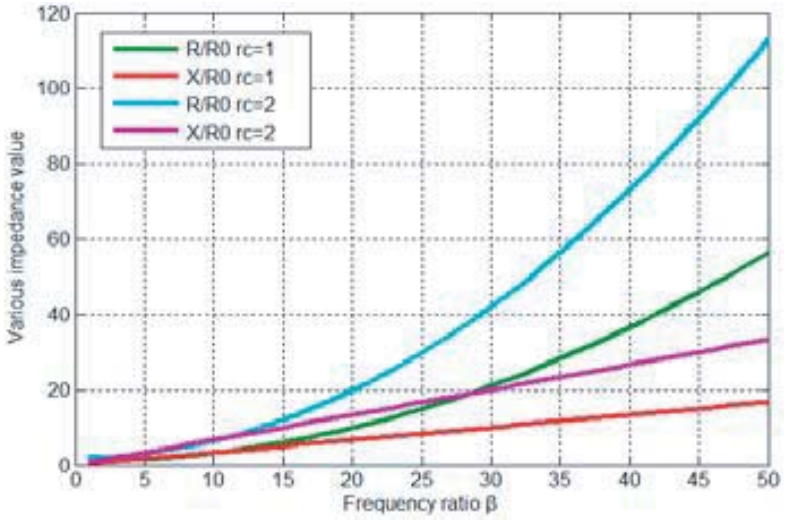

Figure 3. Various impedance value with different frequency ratio β and radius r_c.

Considering the influence of space coupled electromagnetic field around circuit loop on circuit parameters, the change of line impedance is shown as Eq. (17),

$$\begin{cases} \Delta Z_y(r,s) = \dfrac{B_1}{2\pi r_c A_1} \dfrac{\dfrac{\mu s y^2}{(\sigma+\varepsilon s)}}{(len1/2-|y|)} \left(-len2/2 \le y \le len2/2\right) \\ \Delta Z_x(r,s) = \dfrac{B_1}{2\pi r_c A_1} \dfrac{\dfrac{\mu s x^2}{(\sigma+\varepsilon s)}}{(len2/2-|x|)} \left(-len1/2 \le x \le len1/2\right) \\ \Delta I = 4\pi r_c A_1 \sin\theta \dfrac{\sqrt{\sigma\mu s+\varepsilon\mu s^2}\left(|x|-|y|\right)}{\mu s r} \sinh\left(\sqrt{\sigma\mu s+\varepsilon\mu s^2} r\right) \\ \Delta V = \Delta Z \cdot \Delta I \\ V^* = V_0\text{-}\Delta V \\ I^* = I_0\text{-}\Delta I \end{cases} \tag{17}$$

In Eq. (17), the change in impedance is independent of θ, so the following analysis considers $\sin\theta = 1$. When characteristic frequency $\omega_c = 1/\mu\sigma$, make $\beta = \omega/\omega_c = 1$ and $\varepsilon = 0$ at high frequency, and the changes of line impedance, voltage, and current are as follows,

$$\begin{cases} \Delta Z_y(y,\beta) = j\dfrac{B_1}{2\pi r_c A_1 \sigma^2} \dfrac{\beta y^2}{(len1/2-|y|)} \left(-len2/2 \le y \le len2/2\right) \\ \Delta Z_x(x,\beta) = j\dfrac{B_1}{2\pi r_c A_1 \sigma^2} \dfrac{\beta x^2}{(len2/2-|x|)} \left(-len1/2 \le x \le len1/2\right) \\ \Delta I_y = 4\pi r_c A_1 \sigma \dfrac{(len1/2-|y|)}{\sqrt{j\beta}r} \sinh\left(\sqrt{j\beta}r\right) \\ \Delta I_x = 4\pi r_c A_1 \sigma \dfrac{(|x|-len2/2)}{\sqrt{j\beta}r} \sinh\left(\sqrt{j\beta}r\right) \\ \Delta V_y(x,y,\beta) = \dfrac{2B_1}{\sigma} \dfrac{y^2}{(len1/2-|y|)} \cdot \dfrac{j\beta\left(len1/2-|y|\right)}{\sqrt{j\beta}r} \sinh\left(\sqrt{j\beta}r\right) \\ \Delta V_x(x,y,\beta) = \dfrac{2B_1}{\sigma} \dfrac{x^2}{(len2/2-|x|)} \dfrac{j\beta\left(|x|-len2/2\right)}{\sqrt{j\beta}r} \sinh\left(\sqrt{j\beta}r\right) \end{cases} \tag{18}$$

$$\frac{\sinh\lambda}{\lambda} = 1 + \lambda^2/3! + \lambda^4/5! + \lambda^6/7! + \cdots \tag{19}$$

In Fig. 4, the voltage change of line impedance is proportional to $|x|^2 + |y|^2$ and frequency; the current change of line impedance is proportional to $(\|y|-|x\|)*(|x|^2+|y|^2)$ and frequency; the change of line impedance is proportional to $(|x|^2+|y|^2)/(\|y|-|x\|)$ and frequency. It can be seen that changing line impedance at different locations can optimize the influence of space coupled electromagnetic field around circuit loop on circuit parameters, which can reduce spurious parameter loss and improve efficiency.

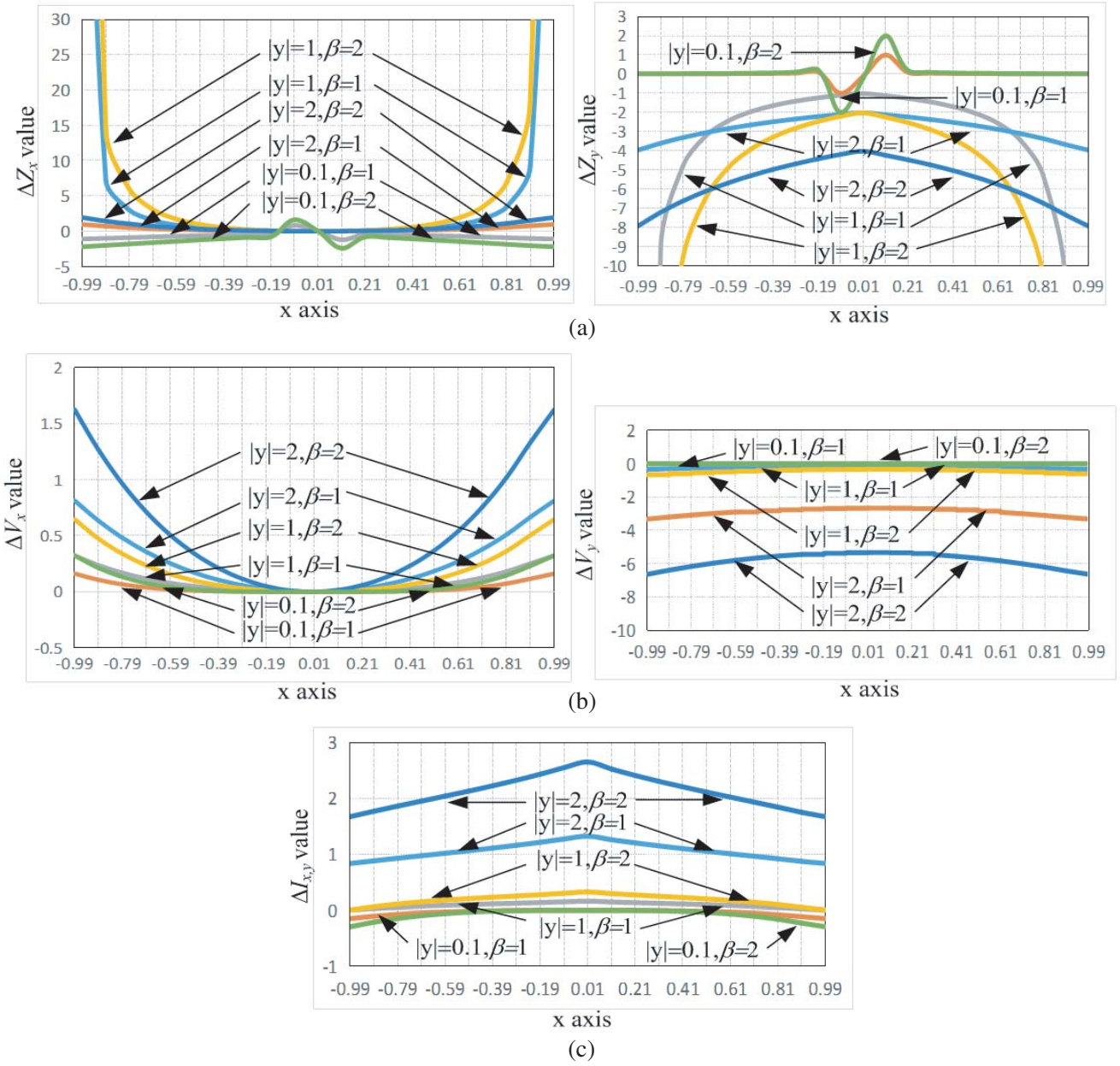

Figure 4. The voltage and current changes of line impedance at different location and frequency. (a) ΔZ_x and ΔZ_y. (b) ΔV_x and ΔV_y. (c) ΔI.

According to the above analysis, the circuit loop l_3-l_2-l_1 in Fig. 5, when $|\Delta x_{1,2}| = |\Delta y_{1,2}| \neq 0$, $|\Delta y_{1,2}| > |\Delta x_{1,2}| = 0$, and $|\Delta x_{1,2}| > |\Delta y_{1,2}| = 0$, radius r and the voltage change of x and y axis ($\Delta\mathbf{E}_x$, $\Delta\mathbf{E}_y$) gradually increase in three ways.

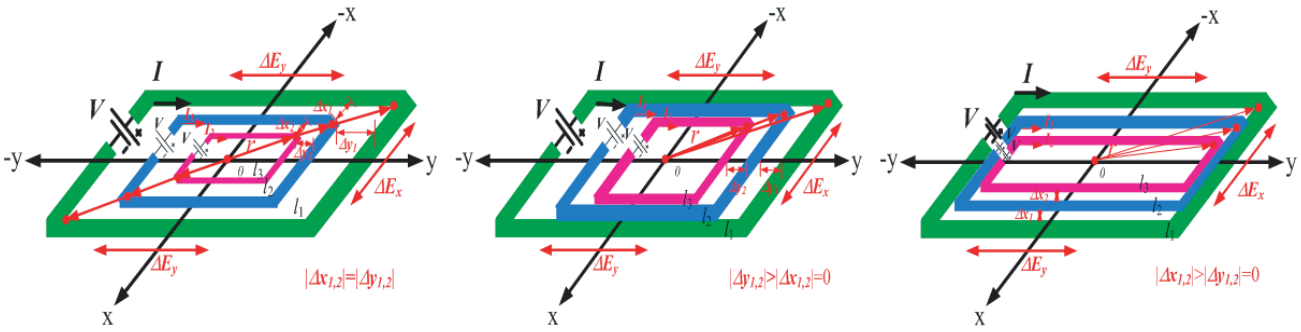

Figure 5. Various line impedance of a circuit loop at different locations.

However, the changes of ΔV_x and ΔV_y are different by three ways. Because the current change of line impedance is proportional to $(\|y| - |x\|) * (|x|^2 + |y|^2)$ and frequency, when $|\Delta y_{1,2}| > |\Delta x_{1,2}| = 0$, $|\Delta x_{1,2}| > |\Delta y_{1,2}| = 0$ and $|\Delta x_{1,2}| \neq |\Delta y_{1,2}|$ and the changes of ΔV_x and ΔV_y are greater than the changes when $|\Delta x_{1,2}| = |\Delta y_{1,2}| \neq 0$.

So changing line impedance at different locations can optimize the voltage and current changes affected by space coupled electromagnetic field around circuit loop.

3. SIMULATION RESULTS VERIFICATION

The following utilizes boost circuit and buck circuit topology in Fig. 6 to verify the correctness and effectiveness of above theoretical analysis.

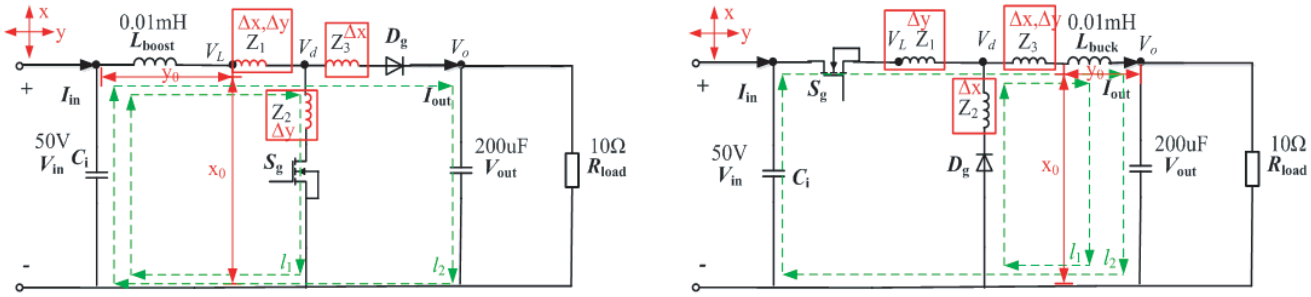

Figure 6. Boost circuit and buck circuit topology with various line impedance at different location.

The results are summarized in Fig. 7, when $Z_1 = Z_2 = Z_3 = 0$ in boost circuit. $V_L = V_d$ is inversely proportional to frequency when $0\,\text{kHz} \leq f_s \leq 50\,\text{kHz}$, which is proportional to frequency when $50\,\text{kHz} \leq f_s \leq 500\,\text{kHz}$. V_o is inversely proportional to frequency. Switching loss is proportional to frequency, and the output current and diode loss are inversely proportional to frequency. When $Z_1 = Z_2 = Z_3 = 50\,\text{n}$, $200\,\text{n}$, $500\,\text{n}$, V_L and V_d are proportional to frequency and impedance value; V_o is inversely proportional to frequency and impedance value. The output current and diode loss are inversely proportional to frequency and impedance value. When $Z_1 = Z_2 = Z_3 = 200\,\text{n}$, switching loss is proportional to frequency when $0\,\text{kHz} \leq f_s \leq 50\,\text{kHz}$; switching loss is inversely proportional to frequency when $50\,\text{kHz} \leq f_s \leq 500\,\text{kHz}$; when $Z_1 = Z_2 = Z_3 = 500\,\text{n}$, switching loss is inversely proportional to frequency.

It can be seen from the above analysis that the output efficiency of boost circuit is related to impedance value and switching frequency. When $Z_1 = Z_2 = Z_3$ increase, the switching loss is inversely proportional to frequency, and efficiency tends to be maximum in high frequency.

When $Z_1 \neq Z_2$, $Z_2 \neq Z_3$, $Z_1 \neq Z_3$, change the values of Z_1, Z_2, Z_3, respectively, and compare the V_L, V_d, V_o difference with $Z_1 = Z_2 = Z_3 = 50\,\text{n}$.

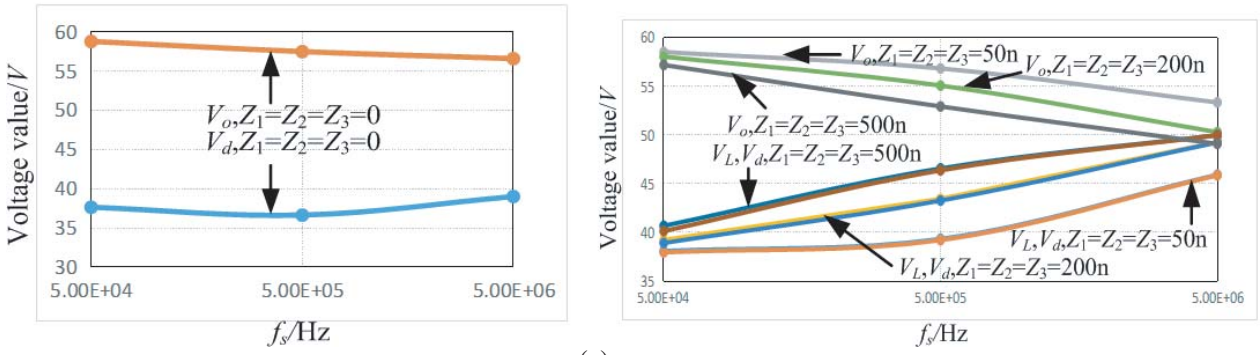

(a)

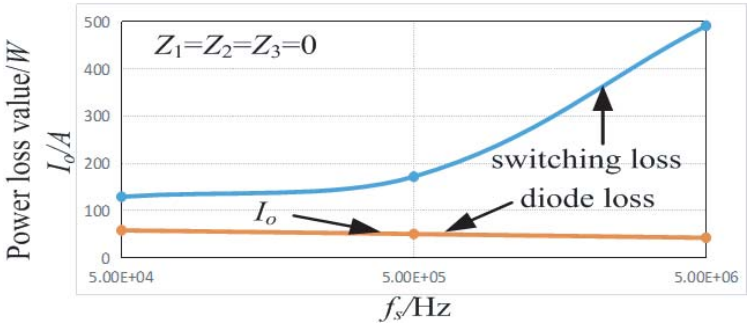

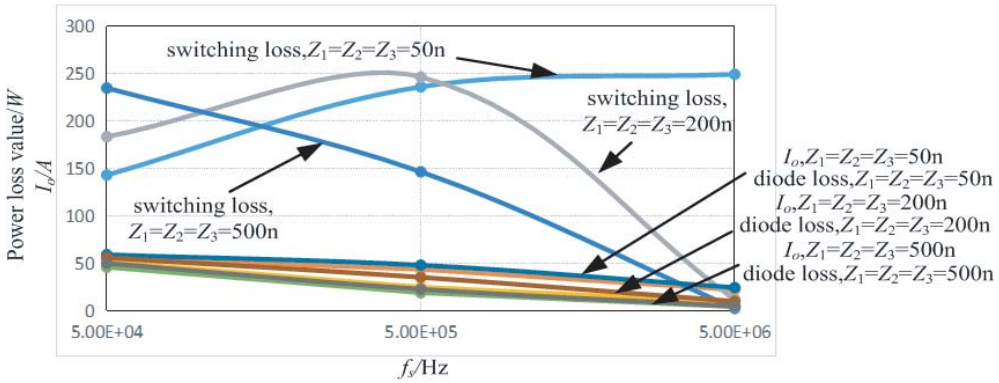

(b)

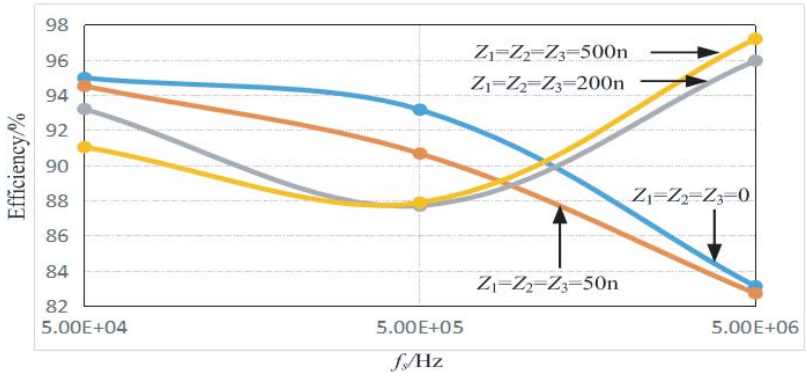

(c)

Figure 7. The changes of various variables with different line impedance and frequency in boost circuit. (a) V_L, V_d and V_o. (b) Power loss value. (c) Efficiency.

It can be seen from Fig. 8 that when Z_2 and Z_3 increase, the voltage difference is more obvious, and the change of Z_1 has less effect on voltage change. The change of voltage conforms to the law analyzed in Fig. 4 and Fig. 5.

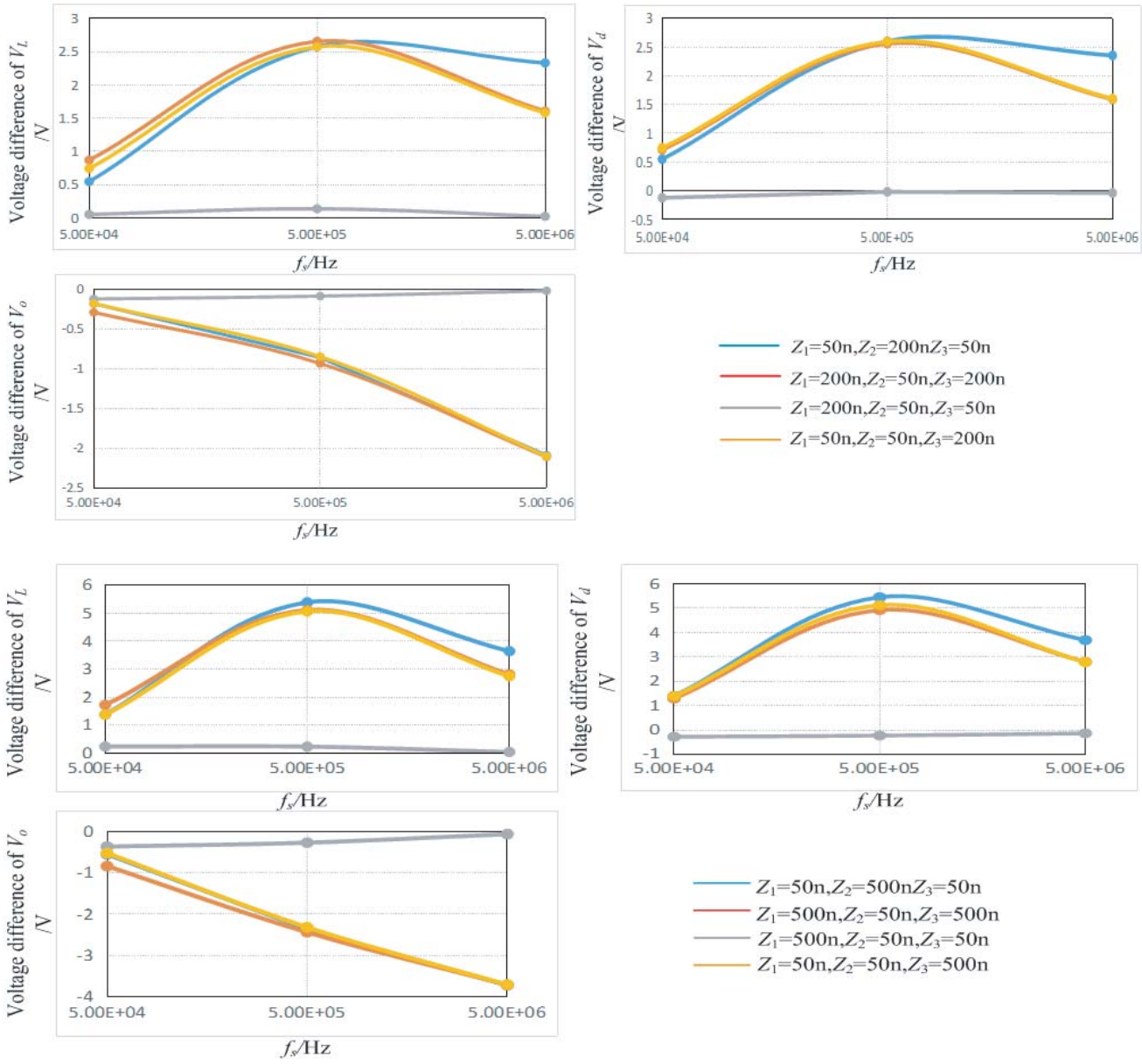

Figure 8. The V_L, V_d and V_o changes of boost circuit with $Z_1 \neq Z_2$, $Z_2 \neq Z_3$, $Z_1 \neq Z_3$.

The results are summarized in Fig. 9, when $Z_1 = Z_2 = Z_3 = 0$ in buck circuit. $V_L = V_d$ is inversely proportional to frequency; V_o is inversely proportional to frequency. Switching loss is proportional to frequency, and the output current and diode loss are inversely proportional to frequency. When $Z_1 = Z_2 = Z_3 = 50\,\text{n}$, 200 n, 500 n, V_L and V_d are inversely proportional to frequency and impedance value; V_o is inversely proportional to frequency and impedance value. The output current and diode loss are inversely proportional to frequency and impedance value. When $Z_1 = Z_2 = Z_3 = 200\,\text{n}$, switching loss is proportional to frequency when $0\,\text{kHz} \leq f_s \leq 50\,\text{kHz}$; switching loss is inversely proportional to frequency when $50\,\text{kHz} \leq f_s \leq 500\,\text{kHz}$; when $Z_1 = Z_2 = Z_3 = 500\,\text{n}$, switching loss is inversely proportional to frequency.

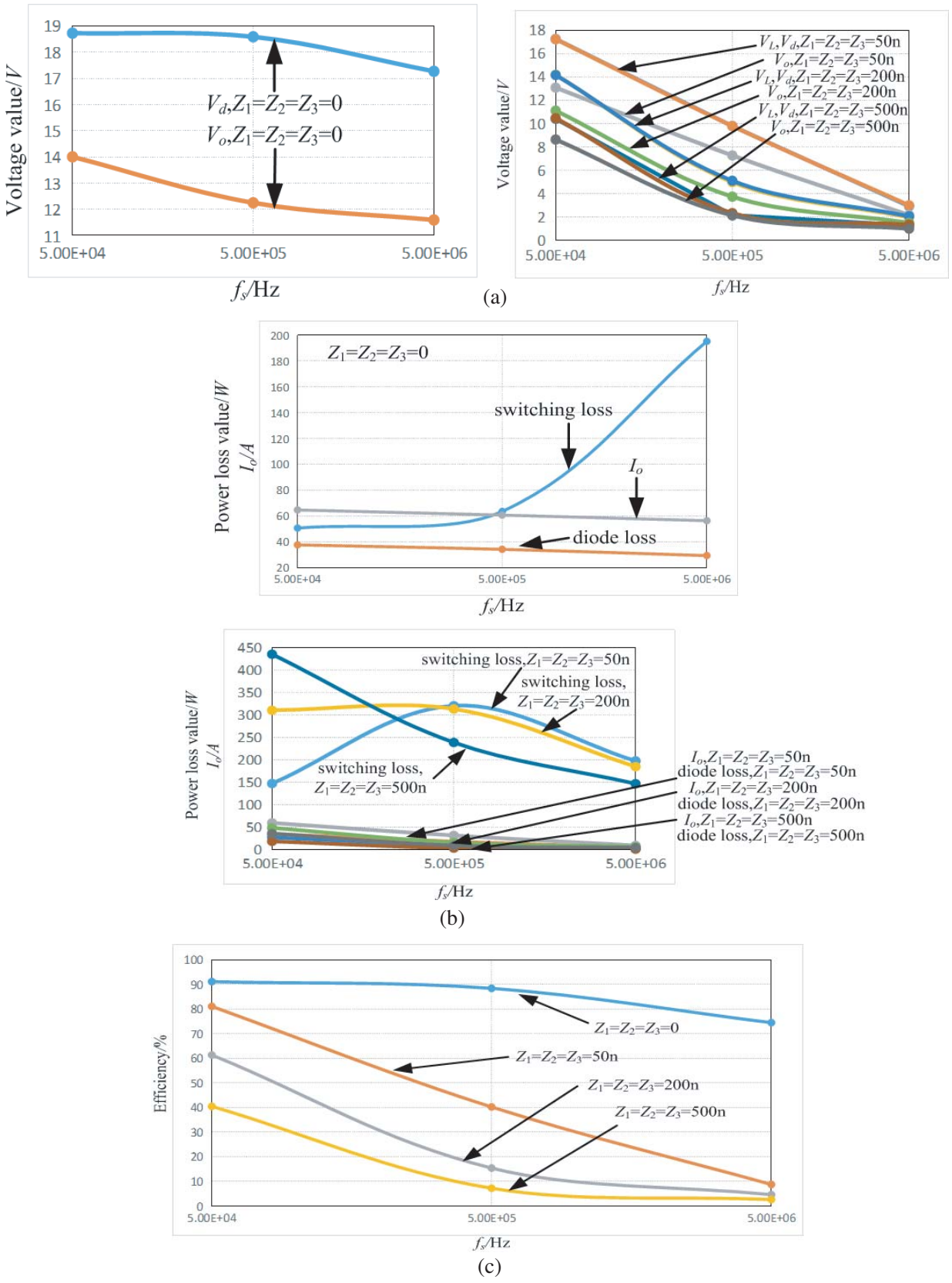

Figure 9. The changes of various variables with different line impedance and frequency in buck circuit. (a) V_L, V_d and V_o. (b) Power loss value. (c) Efficiency.

It can be seen from the above analysis that the output efficiency of buck circuit is related to impedance value and switching frequency. When $Z_1 = Z_2 = Z_3$ increase, the switching loss is inversely proportional to frequency, and efficiency tends to be minimum in high frequency.

When $Z_1 \neq Z_2$, $Z_2 \neq Z_3$, $Z_1 \neq Z_3$, change the values of Z_1, Z_2, Z_3, respectively, and compare the V_L, V_d, V_o difference with $Z_1 = Z_2 = Z_3 = 50\,\text{n}$.

It can be seen from Fig. 10 that when Z_1 and Z_2 increase, the voltage difference is more obvious, and the change of Z_3 has less effect on voltage change. The change of voltage conforms to the law analyzed in Fig. 4 and Fig. 5.

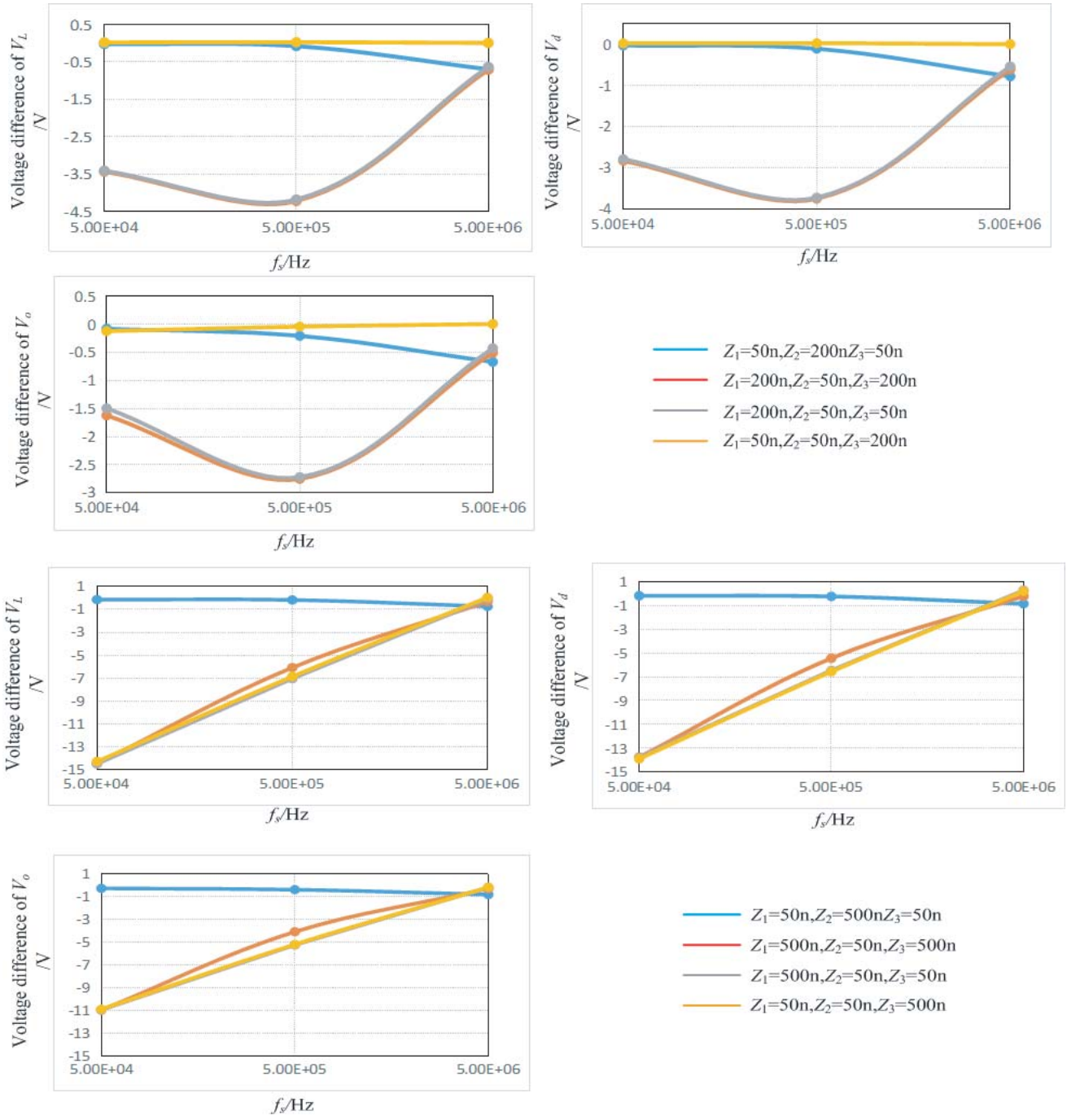

Figure 10. The V_L, V_d and V_o changes of buck circuit with $Z_1 \neq Z_2$, $Z_2 \neq Z_3$, $Z_1 \neq Z_3$.

4. COMPARISON RESULTS VERIFICATION

Compare average voltage difference with the proposed method and simulation results under $Z_1 \neq Z_2$, $Z_2 \neq Z_3$, $Z_1 \neq Z_3$, and $Z_1 = Z_2 = Z_3$ condition, and the comparison results are shown in Fig. 11 and Fig. 12.

In Fig. 11 and Fig. 12, when Z_1, Z_2, and Z_3 increase from 50 n to 500 n, the voltage difference is more obvious; V_d is more obvious than that of V_L and V_o. The voltage changes of nodes are different

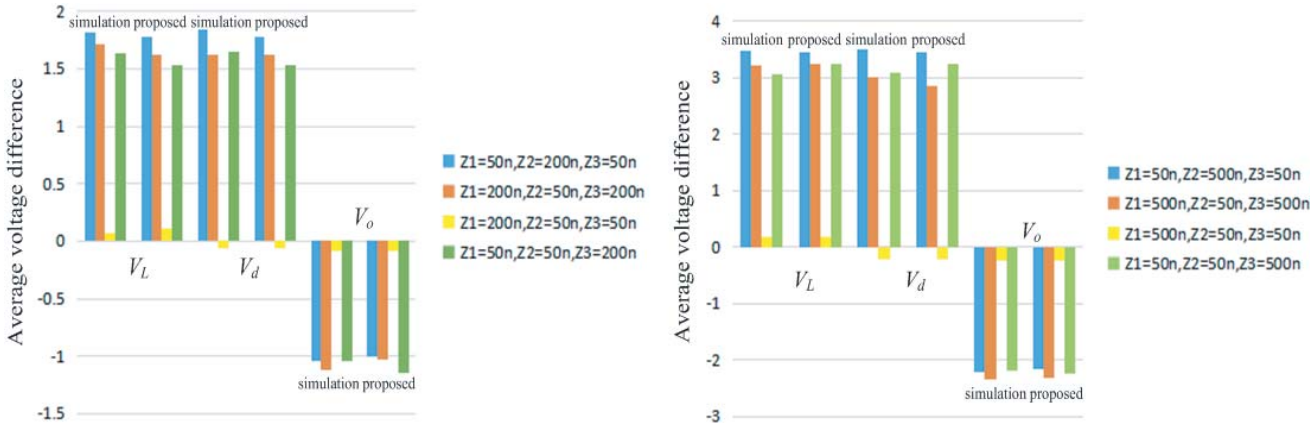

(a)

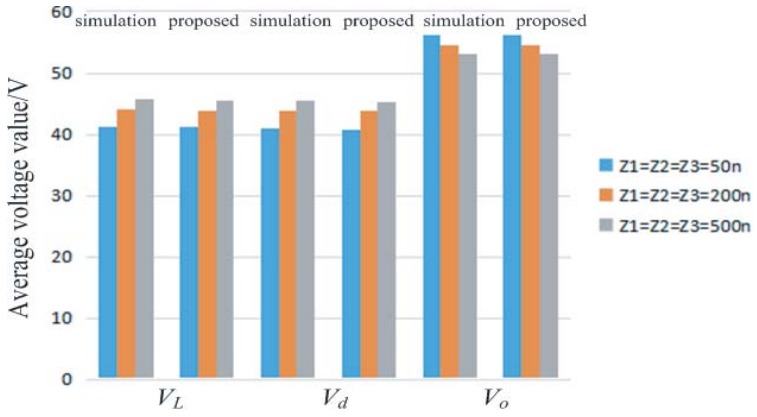

(b)

Figure 11. The V_L, V_d and V_o changes of boost circuit with $Z_1 \neq Z_2$, $Z_2 \neq Z_3$, $Z_1 \neq Z_3$ and $Z_1 = Z_2 = Z_3$. (a) $Z_1 \neq Z_2$, $Z_2 \neq Z_3$, $Z_1 \neq Z_3$ in boost circuit. (b) $Z_1 = Z_2 = Z_3$ in boost circuit.

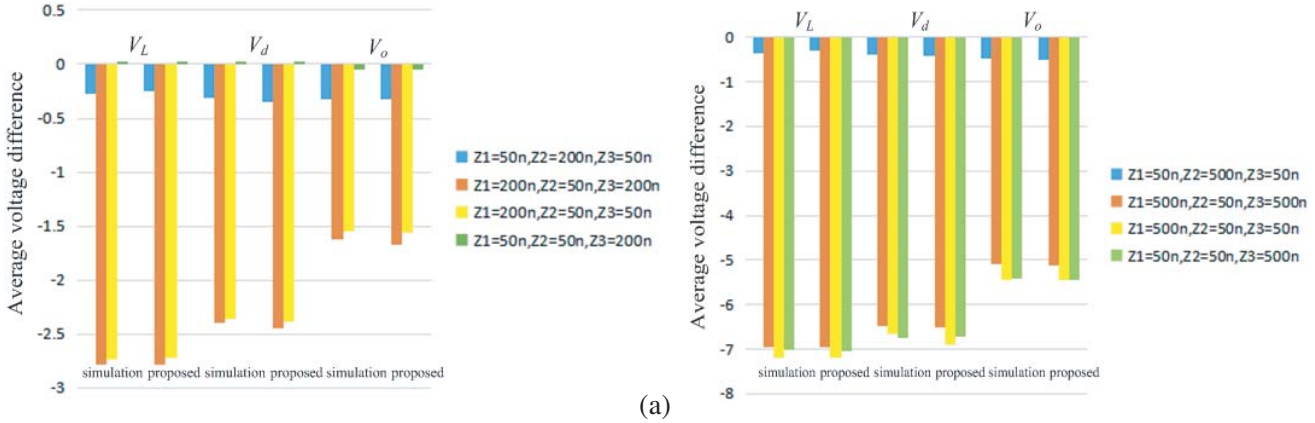

(a)

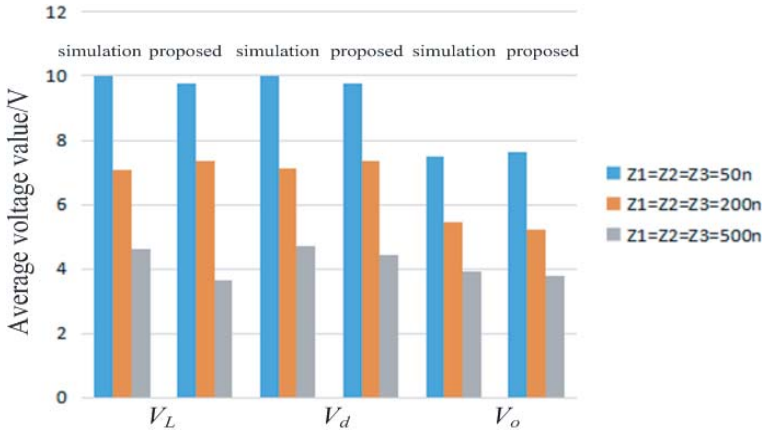

(b)

Figure 12. The V_L, V_d and V_o changes of buck circuit with $Z_1 \neq Z_2$, $Z_2 \neq Z_3$, $Z_1 \neq Z_3$ and $Z_1 = Z_2 = Z_3$. (a) $Z_1 \neq Z_2$, $Z_2 \neq Z_3$, $Z_1 \neq Z_3$ in buck circuit. (b) $Z_1 = Z_2 = Z_3$ in buck circuit.

and affected by space coupled electromagnetic field at different frequencies. So changing line impedance at different locations can optimize the voltage and current changes. Therefore, the analysis of the relationship between space electromagnetic field and voltage and current changes in high-frequency circuit is beneficial to the calculation of node and line voltage changes.

5. CONCLUSION

In high-frequency circuit and parameters optimization of high-frequency converter, the spurious parameters are affected by skin effect and space coupled electromagnetic field changes during switching process. The proposed method based on the relationship between space electromagnetic field and voltage, and current changes in high-frequency circuit. Changing line impedance at different locations can optimize the influence of space coupled electromagnetic field around circuit loop on the voltage and current changes. In addition, changing line impedance at different locations can optimize the influence of space coupled electromagnetic field around circuit loop on circuit parameters and improve efficiency.

In high-frequency circuit and high-frequency converter, the space coupled electromagnetic field distribution is related to switching frequency and affects converter efficiency and power loss. The optimal switching frequency and control time can further optimize efficiency and simplify control process.

REFERENCES

1. Giacoletto, L. J., "Frequency and time-domain analysis of skin effects," *IEEE Transactions on Magnetics*, Vol. 32, No. 1, 1996.
2. Stoll, R. L., *Analysis of Eddy Currents*, Clarendon Press, Oxford, U.K., 1974.
3. Deswal, D. and F. de Leon, "Generalized circuit model for eddy current effects in multi-winding transformers," *IEEE Transactions on Power Delivery*, Vol. 34, No. 2, 2019.
4. Kakhki, M. T., J. Cros, and P. Viarouge, "New approach for accurate prediction of eddy current losses in laminated material in the presence of skin effect with 2-D FEA," *IEEE Transactions on Magnetics*, Vol. 52, No. 3, 2016.
5. Lee, J.-H., N. M. Iyer, and H. Zhang, "Influence of skin effect on the current distribution of grounded-gate NMOS device," *IEEE Electron Device Letters*, Vol. 38, No. 11, 2017.
6. Oh, K. S., "Accurate transient simulation of transmission lines with the skin effect," *IEEE Transactions on Computer-Aided Design of Integrated Circuits and Systems*, Vol. 19, No. 3, 2000.

7. Ney, M. M. and G. I. Costache, "Transient striction and skin effects on voltage drop across flat conductors," *Canadian Journal of Electrical and Computer Engineering*, Vol. 18, No. 4, 1993.
8. Coperich, K. M., A. E. Ruehli, and A. Cangellaris, "Enhanced skin effect for Partial-Element Equivalent-Circuit (PEEC) models," *IEEE Transactions on Microwave Theory and Techniques*, Vol. 48, No. 9, 2000.
9. Haas, H. and F. Schmoellebeck, "A finite-element method for transient skin effect in 2-D loaded multiconductor systems," *IEEE Transactions on Magnetics*, Vol. 24, No. 1, 1988.
10. Vu Dinh, T., B. Cabon, and J. Chilo, "New skin-effect equivalent circuit," *Electronics Letters*, Vol. 26, No. 19, 1990.
11. Sato, K., N. Shinohara, and T. Naito, "A new transient analysis method of the electrical circuit containing with Skin Effect Element (SIC)," *IEEE Transactions on Magnetics*, Vol. 26, No. 2, 1990.
12. Ney, M. M., "Striction and skin effects on the internal impedance value of flat conductors," *IEEE Transactions on Electromagnetic Compatibility*, Vol. 33, No. 4, 1991.
13. Morisco, D. P., S. Kurz, H. Rapp, and A. Möckel, "A hybrid modeling approach for current diffusion in rectangular conductors," *IEEE Transactions on Magnetics*, Vol. 55, No. 9, 2019.
14. Bai, F., Z. Niu, and D. Zhou, "Modeling and simulation of near-field radiation of power converters," *Journal of System Simulation*, Vol. 18, No. 2, 2006.